SAND2013-10756C

Pressure Loading Within Rectangular Cavities With and Without a Captive Store

Matthew Barone*, Srinivasan Arunajatesan†
Sandia National Laboratories‡, Albuquerque, NM 87185

Simulations of a rectangular cavity containing a model captive store are performed using a Hybrid Reynolds-averaged Navier-Stokes/Large Eddy Simulation (RANS/LES) model. The fluid flow simulations are coupled to a structural dynamics finite element model using a one-way pressure transfer procedure. Simulation results for pressure fluctuation spectra and store acceleration are compared to measurements made on the same configuration in a tri-sonic wind tunnel at Mach numbers of 0.60, 0.80, and 1.47. The simulation results are used to calculate unsteady integrated forces and moments acting on the store. Spectra of the forces and moments reveal that a complex relationship exists between the unsteady integrated forces and the measured resonant cavity modes as indicated in the cavity wall pressure measurements. Predictions of the store accelerations from the coupled model show some success in predicting both forced and natural modal responses of the store within the cavity environment, while also highlighting some challenges in obtaining statistically converged results for this class of problems.

I. Introduction

Compressible cavity flows have been extensively studied over the past half-century since the seminal work of Rossiter.[1] The majority of research studies have focused on empty cavities of simple, usually rectangular, geometrical configuration. In many real applications involving cavity flows, such as flow past an aircraft weapons bay, the cavity is neither empty nor of simple geometrical shape.

The Weapons Internal Carriage and Separation (WICS) database[2] included measurements of store and cavity surface pressure fluctuations for a cavity containing a representative, sting-mounted, model store. For these measurements, the length-to-depth ratio of the cavity, or L/D, was 4.5, and Mach numbers ranged from 0.6 to 1.2. The presence of the store resulted in a decrease in amplitude of the primary cavity modes of 2 to 5 dB, and a positive shift in primary mode frequencies of approximately 50 to 100 Hz, which the authors attributed to an "acoustic shortening" of the cavity due to the presence of the model sting.

More recently, Sandia National Laboratories has carried out a series of experiments in the Sandia Trisonic Wind Tunnel (TWT), investigating empty rectangular cavities as well as cavities with a model captive store.[3,4] The measurements with a captive store include cavity unsteady pressure loading as well as simultaneous store acceleration response measurements, providing a rich data set for validation of coupled fluid/structure simulations of such flows.

Computational studies that include a store within a cavity or weapons bay include that of Shipman *et al.*,[5] who investigated the effects of cavity flow control techniques on store loadings and release trajectories for a non-rectangular weapons bay cavity with a generic store body. This study focused on the effects of flow control techniques, rather than on details of the store loading in a captive-carry configuration.

Unsteady pressure loads on a captive store have been studied using hybrid RANS/LES simulations[6] for one of the cavity geometries measured in the WICS campaign. In this particular configuration, the store had only minor effects on the cavity tone amplitudes and frequencies. The simulations revealed that unsteady pressure forces on the store surface correlated very well with single-point pressure spectra measured on the

*Aerosciences Department, Associate Fellow AIAA
†Aerosciences Department, Senior Member AIAA
‡Sandia National Laboratories is a multi-program laboratory managed and operated by Sandia Corporation, a wholly owned subsidiary of Lockheed Martin Corporation, for the U.S. Department of Energy's National Nuclear Security Administration under contract DE-AC04-94AL85000.

cavity walls. Spectra of the store surface longitudinal and vertical force fluctuations, as well as the pitching moment, showed peaks corresponding to cavity tone peaks, while lateral force, yaw moment, and roll moment fluctuations were negligible.

In this work we consider flow past rectangular cavities containing a model store and attempt predictions, using a hybrid RANS/LES CFD model, of the aero-acoustic pressure loading on the store and the resulting structural dynamical response. The cavity and store geometry matches that of the Sandia TWT experiments.[3,4] In a previous paper,[7] the authors demonstrated a coupled fluid-structure simulation of this cavity-with-store configuration at a single supersonic flow condition. In this paper, we present validation results of both empty cavity and cavity-with-store simulations over a range of Mach numbers, and examine details of the pressure loading and resulting store response at each flow condition.

II. Simulation Method

The cavity fluid flow is simulated using the SIGMA CFD[a] code, a multi-block, structured grid, compressible flow solver. The details of this flow solver can be found in a previous paper.[7] The numerical method is formally second order accurate in time and in space; however, the finite volume scheme employs expanded stencils for constructing the inviscid fluxes, resulting in improved accuracy over standard second order constructions.

For the present simulations, the finite volume scheme is a newly implemented hybrid scheme consisting of separate centered and dissipative operators. In keeping with a structured grid implementation, the flux at any face $F_{i+1/2,j,k}$ is evaluated as the sum of a central difference contribution and an upwind biased dissipative contribution,

$$F_{i+1/2,j,k} = \frac{1}{2}\left(F(Q_{i+1,j,k}) + F(Q_{i,j,k})\right) + \sigma_{i+1/2,j,k}F^{O2}_{i+1/2,j,k} + (1-\sigma_{i+1/2,j,k})F^{O5}_{i+1/2,j,k} \tag{1}$$

In the above equation, $F^{O2}_{i+1/2,j,k}$ is a second-order limited (TVD) dissipative flux, $F^{O5}_{i+1/2,j,k}$ is fifth-order dissipative flux and, $\sigma_{i+1/2,j,k}$ is sensor that determines the weights of the contributions of the second and fifth order terms to the total dissipative flux. The dissipative fluxes are computed using the dissipative flux term in Roe's approximate Riemann solver. The $F^{O2}_{i+1/2,j,k}$ is given as follows,

$$\begin{aligned}
F^{O2}_{i+1/2,j,k} &= \tfrac{1}{2}\left[\Delta F^{O2-}_{i+1/2,j,k} - \Delta F^{O2+}_{i+1/2,j,k}\right] \\
\Delta F^{O2-}_{i+1/2,j,k} &= R_{i+1/2,j,k}\Lambda^{-}_{i+1/2,j,k}\left[\Delta\alpha_{i+1/2,j,k} - \tfrac{1}{6}\overline{\Delta\alpha_{i+3/2,j,k}} - \tfrac{1}{3}\overline{\overline{\Delta\alpha_{i+1/2,j,k}}}\right] \\
\Delta F^{O2+}_{i+1/2,j,k} &= R_{i+1/2,j,k}\Lambda^{+}_{i+1/2,j,k}\left[\Delta\alpha_{i+1/2,j,k} - \tfrac{1}{3}\overline{\Delta\alpha_{i+1/2,j,k}} - \tfrac{1}{6}\overline{\overline{\Delta\alpha_{i-1/2,j,k}}}\right]
\end{aligned} \tag{2}$$

Following Rai,[8] the fifth order contribution $F^{O5}_{i+1/2,j,k}$ is computed using a wider stencil and without applying a limiter as follows,

$$\begin{aligned}
F^{O5}_{i+1/2,j,k} &= \tfrac{1}{2}\left[\Delta F^{O5-}_{i+1/2,j,k} - \Delta F^{O5+}_{i+1/2,j,k}\right] \\
\Delta F^{O5-}_{i+1/2,j,k} &= R_{i+1/2,j,k}\Lambda^{-}_{i+1/2,j,k}\left[\tfrac{1}{30}\Delta\alpha_{i+5/2,j,k} - \tfrac{11}{60}\Delta\alpha_{i+3/2,j,k} + \tfrac{1}{10}\Delta\alpha_{i+1/2,j,k} + \tfrac{1}{20}\Delta\alpha_{i-1/2,j,k}\right] \\
\Delta F^{O5+}_{i+1/2,j,k} &= R_{i+1/2,j,k}\Lambda^{+}_{i+1/2,j,k}\left[-\tfrac{1}{30}\Delta\alpha_{i-3/2,j,k} + \tfrac{11}{60}\Delta\alpha_{i-1/2,j,k} - \tfrac{1}{10}\Delta\alpha_{i+1/2,j,k} - \tfrac{1}{20}\Delta\alpha_{i+3/2,j,k}\right]
\end{aligned} \tag{3}$$

In the above equations $\Delta\alpha$ are the (unlimited) characteristic variables, the overbar terms are limited forms of the characteristic variables - the expressions for these are given below. The min-mod limiter ($\mathrm{minmod(x,y)} = \mathrm{sign(x)}\ \max(0, \min(|\mathrm{x}|, \mathrm{y}\,\mathrm{sign(x)}))$) is used throughout this work.

[a] Sandia Implicit Generalized Multi-Block Analysis Code for Fluid Dynamics

$$\Delta\alpha_{i+1/2,j,k} = L_{i+1/2,j,k}(Q_{i+1,j,k} - Q_{i,j,k})$$

$$\overline{\Delta\alpha_{i+1/2,j,k}} = \text{minmod}(\Delta\alpha_{\text{i+1/2,j,k}}, \beta\Delta\alpha_{\text{i-1/2,j,k}}) \tag{4}$$

$$\overline{\overline{\Delta\alpha_{i+1/2,j,k}}} = \text{minmod}(\Delta\alpha_{\text{i+1/2,j,k}}, \beta\Delta\alpha_{\text{i+3/2,j,k}})$$

The sensor $\sigma_{i+1/2,j,k}$ used in this work is identical to the one proposed by Spalart and co-workers[9] and is omitted here for brevity.

The turbulence model used in the present simulations is the hybrid RANS-LES model described in Arunajatesan and Sinha.[10] This hybrid RANS-LES model has been validated for prediction of empty, rectangular, compressible cavity flows over a range of flow conditions and against data sets from multiple wind tunnel facilities. A subset of the results of these validation studies is included in Arunajatesan *et al.*[7]

For coupled fluid-structure simulations, a one-way coupling scheme is used, where fluid pressures are transferred to nodes of a structural dynamics FEA model at a specified time interval.[11] The structural dynamics solver, Sierra/SD, solves the linear structural dynamics equations in the time domain. Special elements are included to model nonlinearities associated with joints. Verification and validation results for the SIGMA CFD-Sierra/SD coupling have been reported elsewhere.[7, 11]

III. Description of Experiment and Simulation Setup

III.A. Simultaneous Pressure and Response Measurements

The simulations presented in this paper model the series of cavity flow experiments performed recently in the Trisonic Wind Tunnel (TWT) at Sandia National Laboratories. The goals of these experiments were to 1) provide validation data for coupled fluid-structure simulations of weapons bay flows, and 2) investigate the mechanisms of captive store loading within a cavity. The details of these experiments are explained more fully in papers by Wagner *et al.*[3, 4] We give a brief description of the experimental setup and measurements here.

This series of experiments included flow over empty, rectangular cavities as well as cavities containing a model cylindrical store. The cavity was contained in an insert, shown in Figure 1, that was mounted on either the bottom (supersonic) or top (subsonic) wall of the TWT test section. The stream-wise length L, spanwise width W and depth D of the cavity were 127 mm, 127 mm, and 38.1 mm, respectively, giving $L/D = W/D = 3.33$. The hollow, aluminum, cylindrical model store was 108.0 mm ($0.85L$) long, with an outer diameter of 19.1 mm ($0.5D$) and an inner diameter of 9.5 mm. The model store was mounted to the cavity floor with two hollow threaded rods, and was instrumented with two miniature accelerometers, each mounted on flanges bolted to either end of the cylindrical shell. Additionally, unsteady pressure was measured using dynamic pressure sensors located at several locations along the aft wall of the cavity; for supersonic Mach numbers, pressure was also measured on the forward wall of the cavity. For the empty cavity cases, additional pressure measurements were made at several locations along the cavity floor.

The TWT utilizes different test section configurations for subsonic and supersonic testing. For subsonic Mach numbers, the test section has a cross-section measuring twelve inches by twelve inches, and the cavity cutout is inserted into the top test section wall. For supersonic Mach numbers, the test section height is reduced to six inches, and the cavity cutout is inserted into the bottom wall. No acoustical treatments were applied to the wind tunnel walls during this set of experiments. The simulation domain includes the test section walls in order to account for any possible cavity/test section interactions.

III.B. Fluid Simulation Setup

The subsonic simulations were performed on a computational domain that extends three cavity lengths upstream of the cavity lip and three cavity lengths downstream of the cavity. For the supersonic case, the inflow boundary is only one cavity length upstream of the cavity lip. Proper enforcement of boundary conditions is essential for capturing the correct flow response within the cavity. First, a steady RANS solution was obtained for the flow within the empty TWT, including the region just downstream of the wind tunnel plenum as well as the entire converging-diverging nozzle and test section. This solution was used to determine the back pressure required for matching the tunnel free stream Mach number for subsonic

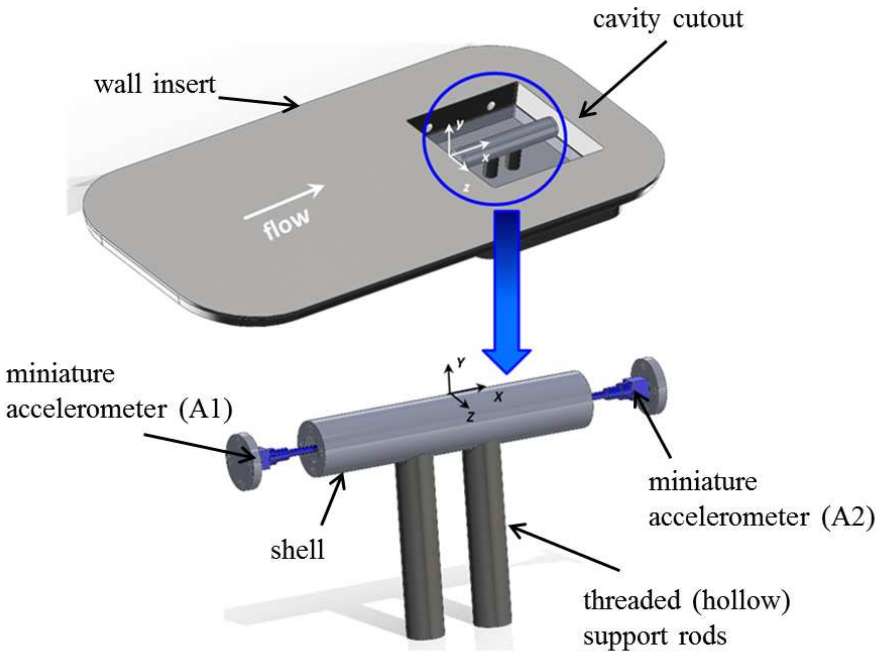

Figure 1. Schematic of the Cavity-with-store wind tunnel experiment.

cases, as well as the inflow boundary layer profile for the cavity simulations. The turbulent boundary layer along the wall opposite the cavity was modeled, while slip wall conditions were applied on the lateral tunnel walls. Sponge zone boundary conditions were applied upstream (for the subsonic cases) and downstream of the cavity in order to absorb radiating acoustic waves and convecting turbulent disturbances with minimal spurious wave reflections.

Empty cavity simulations were run for Mach number, M, equal to 0.60, 0.71, 0.80, 0.89, and 1.47, matching the experimental conditions for Mach number, dynamic pressure, and Reynolds number. Cavity-with-store simulations were run for Mach numbers of 0.60, 0.80, and 1.47, also matching the experimental conditions. The computational mesh for the supersonic case was comprised of 86 million cells, while the mesh for the subsonic cases contained approximately 100 million cells. Figure 2 shows the computational domain for the supersonic case, along with the multi-block mesh topology.

The length scale determining the extent of the RANS region close to solid surfaces was set to a uniform value of 2.54 mm. A time step of 2.5×10^{-7} seconds was used for the Mach 1.5 case, while a time step of 5.0×10^{-7} seconds was used for the subsonic cases. Fluid-only simulations were run for at least 225,000 time steps in each case. The fluid-structure coupling was then introduced and the runs were continued. The Mach 0.60 case was run in coupled mode for 190,000 steps, the Mach 0.80 case for 197,000 steps, and the Mach 1.47 case for 272,000 steps. The simulations were run on several high-performance computing platforms at Sandia National Laboratories and sister DOE laboratory facilities. Each fluid simulation was run on up to 4096 cores, while the structural dynamics solver was run in parallel on 65 cores.

IV. Empty Cavity Results

The authors previously reported on a number of validation studies comparing simulation results for empty, rectangular cavity flows with experiments in various wind tunnel facilities.[7] These included comparisons of simulated and measured wall pressure spectra for an empty cavity with $L/D = 3.33$, $L/W = 1$ at $M = 1.47$ in the TWT facility. For completeness, further empty cavity simulation results at several subsonic Mach numbers are presented here.

In Figures 3 and 4, simulated wall pressure spectra on the center of the aft cavity wall are compared with measured spectra for Mach numbers of 0.60, 0.71, 0.80, and 0.89. The frequencies of the spectral peaks, corresponding to the cavity resonant modes, or 'Rossiter modes,' agree with the experiment to within 5 %,

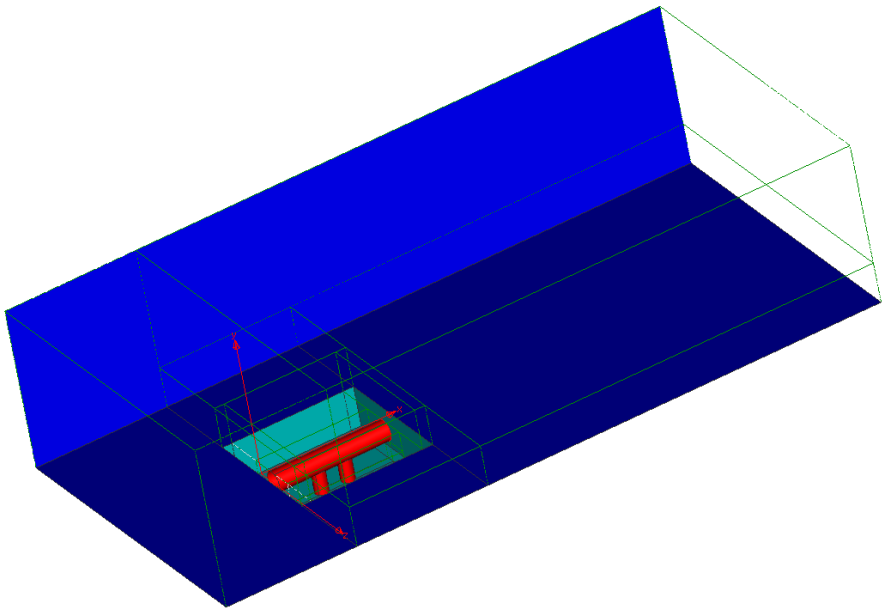

Figure 2. Computational domain with multi-block grid topology for cavity with store simulations.

while the amplitudes of the predominant modes agree to within 5 dB and in most cases to within 2-3 dB. The tails of the simulated spectra (out to 20 kHz) also match the measured spectra quite well, with some deviation evident for the $M = 0.6$ case.

Simulated spectra for other pressure sensor locations on the aft wall and cavity floor (not shown) show similar levels of agreement with measurements. These results, together with the previously reported results for $M = 1.47$,[7] give confidence in the ability of the CFD model to accurately predict aero-acoustic loading within a cavity for both subsonic and supersonic Mach numbers.

V. Cavity with Store Results

In this section we first compare simulated pressure spectra to measured spectra on the cavity walls for the case when the model store is present. We then examine the spectral content and other characteristics of the integrated forces and moments acting on the store. Finally, we present results on the simulated store response and compare these to experimental acceleration measurements.

V.A. Aero-acoustic Pressure Loading

Wall pressure power spectral densities (PSDs) were calculated from simulation pressure signals taken from points where experimental pressure measurements were made. The simulation pressure PSDs were computed using windowed segments of 50,000 samples per segment, with overlap of 0.75 between segments, resulting in a frequency resolution of 40 Hz. The experimental pressure PSDs were processed in an identical fashion.

Figure 5 compares the simulated and measured pressure PSDs at Mach 0.60 for two locations on the aft cavity wall. As noted in Wagner *et al.*,[4] the amplitude of the spectral peaks changes significantly as a result of the presence of the store. For Mach number equal to 0.60, the dominant second Rossiter mode is predicted well by the simulation. At these locations, the amplitude of the first Rossiter mode is underpredicted by about 4.5 dB, while the amplitude of the third Rossiter mode is overpredicted by about 6 dB. While the overall PSD shows reasonable agreement with experiment, accuracy at this Mach number is somewhat degraded relative to the empty cavity PSD shown in Figure 3(a).

Figure 6 shows the same comparison for the Mach 0.80 case. The frequencies of the first three Rossiter modes are slightly overpredicted in the simulation, but the amplitudes are captured to within 2 dB. The simulated fourth mode peak near 3080 Hz appears to be more prominent than the measurements indicate, but the energy associated with this mode is relatively small. The shape of the tail of the PSD closely matches

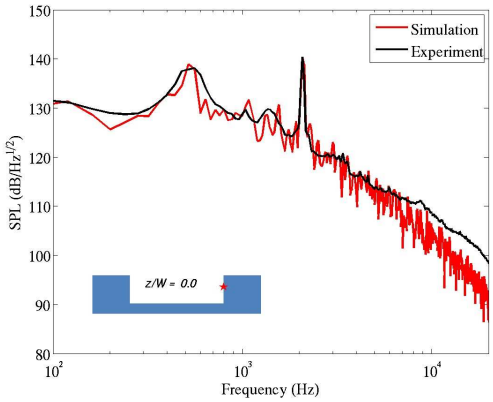

(a) Mach 0.60.

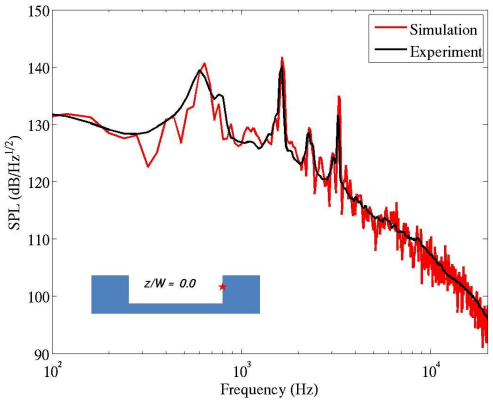

(b) Mach 0.71.

Figure 3. Pressure PSD on the aft cavity wall, empty cavity.

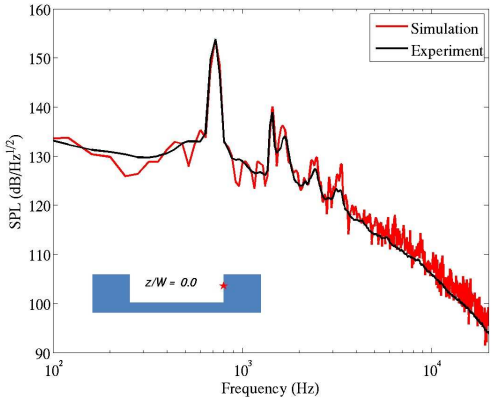

(a) Mach 0.80.

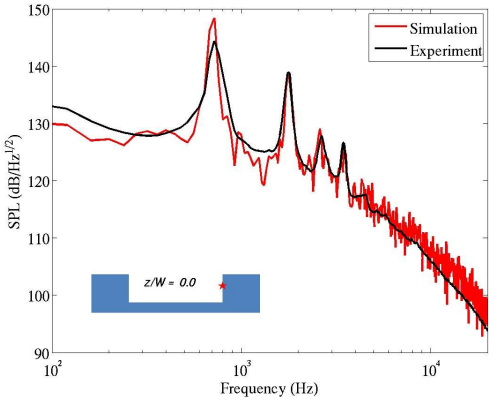

(b) Mach 0.89.

Figure 4. Pressure PSD on the aft cavity wall, empty cavity.

the experimental PSD up to 20 kHz.

For the $M = 1.47$ case, pressure measurements were also made on the forward cavity wall. Figures 7 and 8 show simulated and measured pressure PSDs for locations on the aft and forward cavity wall, respectively. Overall agreement is excellent, with the first four Rossiter mode peaks captured to within 3.5 dB. The fourth mode near 4200 Hz exhibits a double-peak behavior, observed both in the experiment and the simulation. The simulation overpredicts the amplitude of the higher-frequency peak by about 2–5 dB.

Overall, the agreement in these spectra lend confidence that the aero-acoustic loading environment within the cavity and on the store surface is being accurately captured by the simulations.

V.B. Integrated Store Loading

Aerodynamic forces and moments on the store were computed at each time step, allowing the integrated forcing of the store by the flow to be examined. Moments were calculated about the center of mass of the store (including support rods), which was located at $(x, y, z) = (63.2, -11.0, 0)$ mm.

Figure 9 shows PSDs of the force and moment components for $M = 0.60$. The observed Rossiter mode frequencies from the centerline aft wall pressure PSDs are marked by dashed lines in the figures and labeled 'R1', 'R2', etc. The presence or absence of peaks in the force and moment spectra at the Rossiter mode frequencies depends on the force/moment component considered, as well as on the particular mode. The streamwise force has strong spectral peaks at the second and third mode frequencies, and weaker peaks at the first, fourth and fifth modes. The vertical force ($y-$direction) shows peaks at the second, fourth,

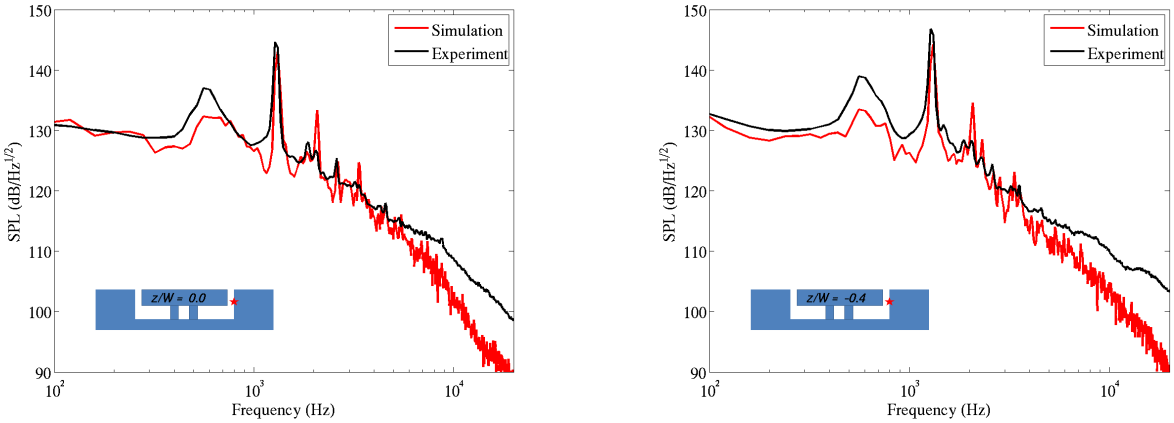

(a) $z/W = 0$. **(b)** $z/W = -0.4$.

Figure 5. Pressure PSD on the aft cavity wall, y/D = −0.42, cavity with store, M = 0.60.

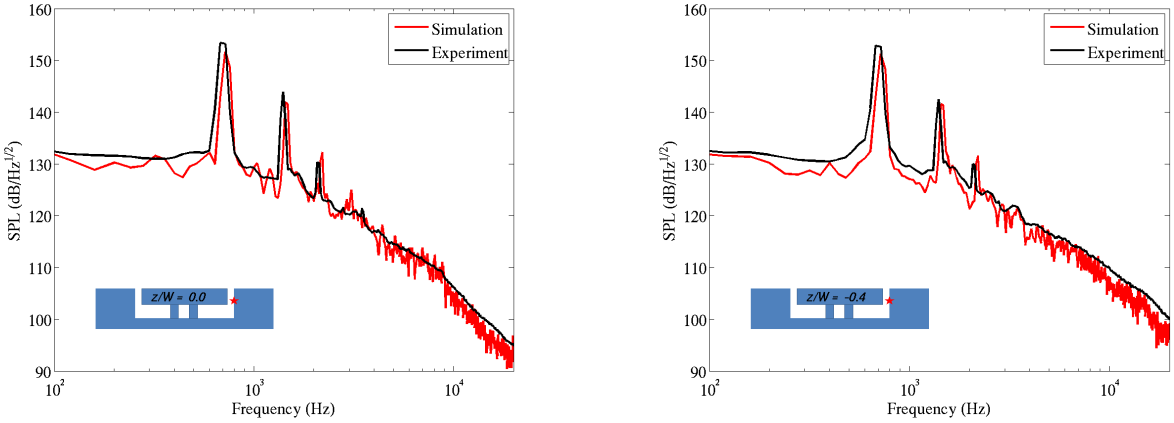

(a) $z/W = 0$. **(b)** $z/W = -0.4$.

Figure 6. Pressure PSD on the aft cavity wall, y/D = −0.42, cavity with store, M = 0.80.

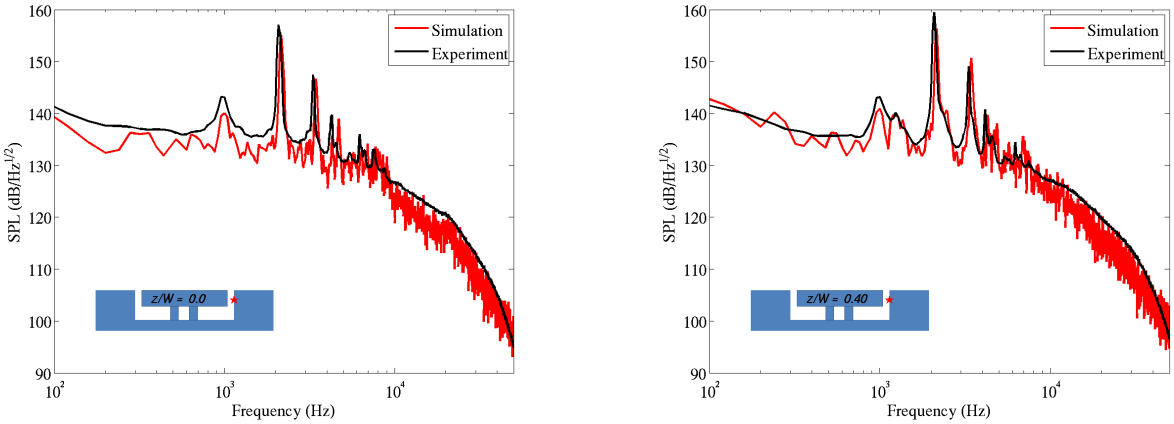

(a) $z/W = 0$. **(b)** $z/W = 0.4$.

Figure 7. Pressure PSD on the aft cavity wall, y/D = −0.33, cavity with store, M = 1.47.

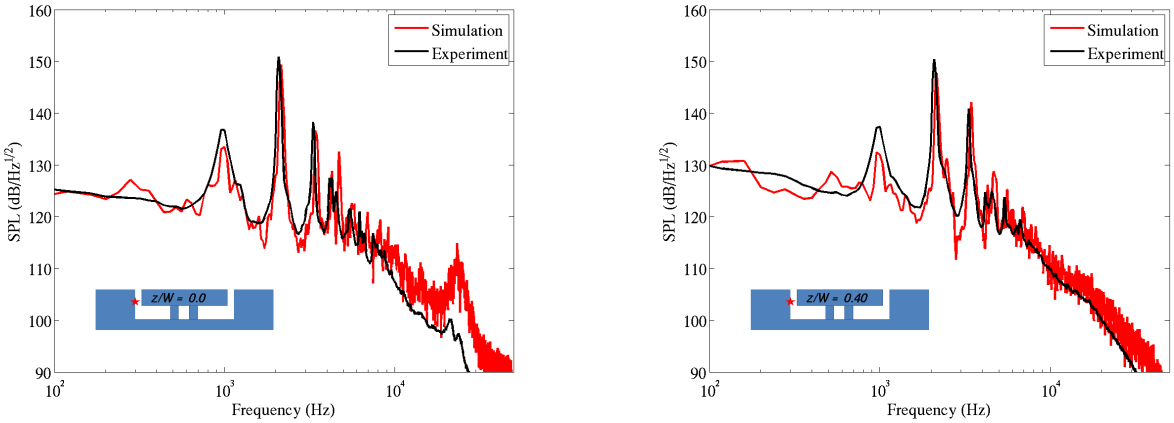

(a) $z/W = 0$. **(b)** $z/W = 0.4$.

Figure 8. Pressure PSD on the forward cavity wall, y/D = −0.63, cavity with store, M = 1.47.

and fifth modes but no peaks at the first and third modes. The lateral (z-direction) force PSD does not contain peaks at the Rossiter mode frequencies, but does contain modest peaks at other frequencies. The moment PSDs for $M = 0.60$ reveal that the roll moment fluctuations are much weaker than the pitch and yaw moment fluctuations; this holds for all Mach numbers simulated. The pitching moment shows peaks at several Rossiter mode frequencies, while the yaw moment only shows a weak peak at the second mode frequency. There is a peak in the yaw moment spectrum at 2320 Hz evidently associated with the peak in the lateral force PSD at the same frequency.

Figure 10 shows the force and moment PSDs for $M = 0.80$. For this Mach number, the streamwise and vertical forces exhibit spectral peaks at the first three Rossiter modes, with the streamwise force peaks at the first two modes dominating the overall force response. There are no force spectral peaks associated with 'R4', although recall that this mode exhibited a double-peaked pressure spectrum (Figure 6(a)), and there are force responses evident at the frequency corresponding to the lower-amplitude pressure spectrum peak. Again, there are peaks evident in the lateral force PSD at frequencies other than the Rossiter mode frequencies, especially evident at 4320 Hz and 7000 Hz. The moment PSDs reveal a strong peak in the pitch moment at the first mode frequency. There are also peaks in pitch moment near the fourth mode and at a higher frequency (3640 Hz). The yaw moment PSD does not exhibit any pronounced peaks, unlike the $M = 0.60$ case.

The force and moment PSDs for $M = 1.47$ are shown in Figure 11. The streamwise and vertical forces both participate in the response at the second and third Rossiter mode frequencies, but with different contribution levels. The streamwise force fluctuations are larger at mode two, while the vertical force fluctuations are larger at mode three. At mode one, only the streamwise force shows a spectral peak. Mode four, which also showed a double-peak in the pressure specturm, shows a force response at the lower-frequency, minor peak. Peaks in the pitch moment at modes two and three and a third peak in between modes three and four dominate the moment spectra. It is interesting to note that the yaw moment contains small peaks at a slightly higher frequency than Rossiter modes two and three.

To summarize, the integrated force and moment spectra show appreciable fluctuation levels for all three force components and the pitch and yaw moments, although the streamwise force, vertical force, and pitch moment exhibit the strongest spectral peaks. Only the rolling moment fluctuations can be considered small compared to the other components. The store forces and moment spectra indicate complex behavior that is not entirely determined by the response at Rossiter mode frequencies. Further, the response at Rossiter mode frequencies, as determined from the aft wall cavity pressure spectrum, does not always correspond to clear responses in vertical and streamwise force fluctuations. This is in contrast to the results of a previous captive store simulation study,[6] where it was found that the streamwise and vertical force spectra were more strongly correlated with the cavity wall pressure spectra. The difference is likely due to the relatively large dimensions of the store and its placement within the cavity shear layer in the present study.

The relationships between the integrated store forces and moments are explored by examining the cor-

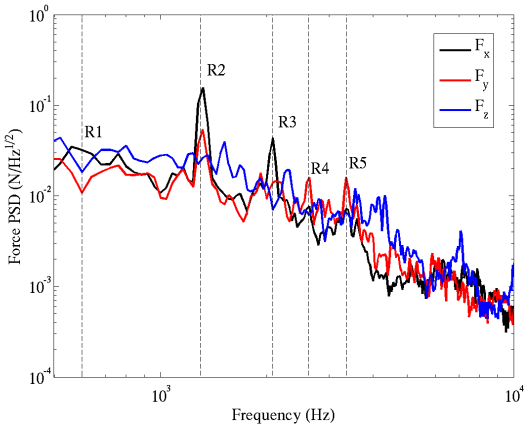

(a) Force PSD.

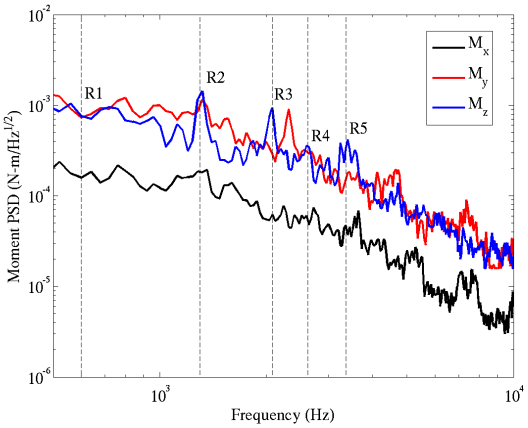

(b) Moment PSD.

Figure 9. Store Force and Moment PSDs, M = 0.60.

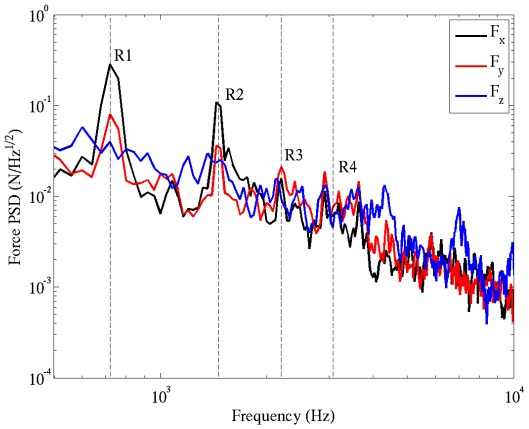

(a) Force PSD.

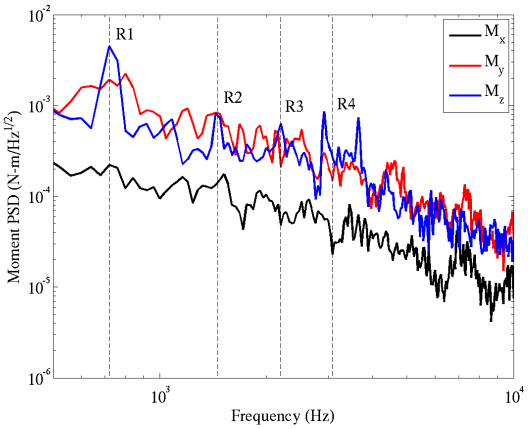

(b) Moment PSD.

Figure 10. Store Force and Moment PSDs, M = 0.80.

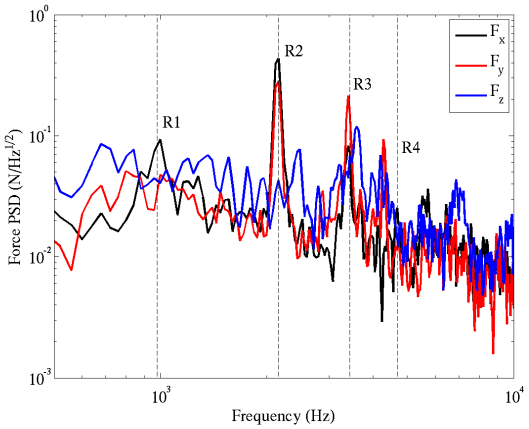

(a) Force PSD.

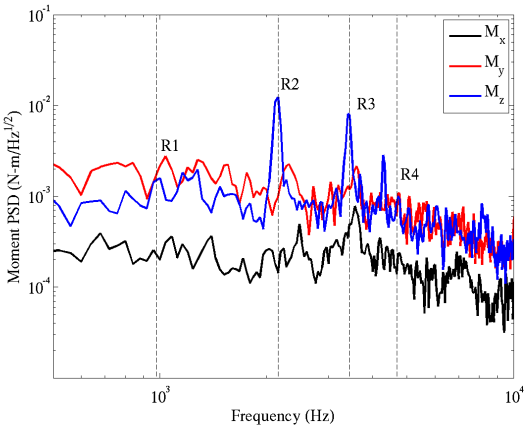

(b) Moment PSD.

Figure 11. Store Force and Moment PSDs, M = 1.47.

relation coefficient calculated between different force and moment pairs. Tables 1 through 3 display the calculated correlation coefficients for each force/moment pair. Some features of the correlations are common across the three Mach numbers. For example, the vertical force is strongly and positively correlated with the pitch moment, and the lateral force is strongly and negatively correlated with the yaw moment. The signs on these two correlations indicate that the forcing is stronger near the aft end of the store than near the front end of the store. The streamwise force is weakly correlated with the yaw moment, indicating that the main contribution to yaw moment is the lateral force.

Other features of the correlations show differences with Mach number. For $M = 0.6$, the streamwise and vertical forces are uncorrelated, while at $M = 0.8$ they are weakly correlated and at $M = 1.47$ they are more strongly correlated. This is consistent with the PSDs presented above, where at $M = 0.6$ the streamwise and vertical force spectra were quite distinct. Another interesting difference as Mach number changes is the correlation between streamwise force and pitch moment. For $M = 0.6$ and $M = 1.47$ this correlation is negative, indicating that the streamwise force acts through a point above the store center of mass. However, for $M = 0.8$ this correlation is positive, indicating the force is acting through a point below the center of mass. Recall that the forces and moments include the contributions from the support posts. It may be that the streamwise force acting on the support posts is greater at $M = 0.8$ than for the other two Mach numbers.

	F_x	F_y	F_z	M_y	M_z
F_x	—				
F_y	−0.03	—			
F_z	−0.03	0.01	—		
M_y	0.04	—	−0.52	—	
M_z	−0.29	0.47	—	0.04	—

Table 1. Correlation coefficients for force/moment signal pairs, M = 0.60.

	F_x	F_y	F_z	M_y	M_z
F_x	—				
F_y	−0.27	—			
F_z	−0.10	−0.01	—		
M_y	0.09	—	−0.55	—	
M_z	0.55	0.43	—	−0.10	—

Table 2. Correlation coefficients for force/moment signal pairs, M = 0.80.

	F_x	F_y	F_z	M_y	M_z
F_x	—				
F_y	−0.51	—			
F_z	−0.09	−0.01	—		
M_y	0.07	—	−0.40	—	
M_z	−0.64	0.67	—	−0.10	—

Table 3. Correlation coefficients for force/moment signal pairs, M = 1.47.

V.C. Store Response Predictions

The one-way coupled fluid-structure simulation method described in Section II was used to simulate the store response to the fluid loading within the cavity for all three Mach numbers. In this paper, we present only results for Mach numbers of 0.80 and 1.47. The results for Mach number of 0.60 were not yet complete and could not be included.

As described in Wagner *et al.*,[4] the store response is a combination of a forced response at Rossiter mode frequencies and a natural response at the store modal frequencies. The store modal frequencies of the structural dynamics model are listed in Table 4. More details on construction of the structural dynamics model are found in Arunajatesan *et al.*[7]

Mode Number	Frequency (Hz)
1	1486
2	1589
3	2091
4	4095
5	4165
6	4583
7	4589
8	4626
9	4740
10	6760
11	8468

Table 4. Modal frequencies for the first eleven modes of the store structural dynamics model.

Figures 12 and 13 show the time histories of the simulated accelerations for the aft accelerometer location (A2) from the experiment. In addition, these figures show the centerline aft cavity wall pressure from the simulation. For $M = 0.80$, the pressure signal appears, qualitatively, to be stationary; *i.e.*, the frequency content and fluctuation amplitude of the pressure signal does not change significantly over the duration of the simulation. The acceleration signals, however, reveal significant amplitude modulation and possibly mode-switching behavior. For $M = 1.47$, the pressure signal appears less stationary than the $M = 0.80$ pressure. There is some evidence that both the frequency content and amplitude of oscillation change with time over the duration of the signal. This may be due to mode-switching; a detailed spectral analysis could reveal if this is the case, but we have not yet performed this analysis. The structural response again reveals amplitude modulation and possibly mode switching or mode interference.

The acceleration time signals raise questions about the statistical convergence of the results for the time period that was simulated. In order to estimate this uncertainty, the RMS of the accelerations was computed using four different subsets of the full time window T, each of length $T/2$ and beginning at $t = 0$, $t = 0.25T$, $t = 0.5T$, and $t = 0.75T$. Periodic continuation of the signal was used to fill out the last subset. The maximum deviation of the RMS acceleration for the four windows is presented as a percentage of the RMS acceleration using the entire simulated signal in Table 5. Longer simulation times are indicated in order to reduce the statistical convergence error, particularly for the x and y accelerations. However, the simulations are already fairly long in terms of number of cavity flow oscillation periods, number of time steps and, most importantly, computational cost.

Keeping in mind that moderate statistical convergence error is present in the results, we present aft store acceleration spectra in Figures 14 and 15. Comparisons for the forward accelerometer location gave similar results. For $M = 0.80$, the measured x and y acceleration peaks at the Rossiter frequencies are present in the predicted PSD. However, the response of the store to the first Rossiter mode near 700 Hz is underpredicted. The measured y acceleration response at 5160 Hz appears to be absent in the simulated spectrum. This response corresponds to store mode Y3, which is a vertical cylinder bending mode. This mode appears in the structural dynamics FEA model at 4165 Hz. Examination of the figure shows a peak corresponding to a simulated response of this mode, albeit at a lower amplitude than was measured. The store response in the z direction is dominated by store modes, with little influence of the cavity mode forcing.[4] The structural modal response near 1500 Hz is well-predicted but the modal response at 6640 Hz is underpredicted. There is also a simulated modal response in z at 8460 Hz that does not appear in the experimental measurement. Similar observations are made for $M = 1.47$, although overall the agreement between simulation and measurement is better at this Mach number.

There are several explanations for the observed discrepancies between the measured and experimental acceleration results. The first is the statistical convergence error previously noted. Secondly, the structural dynamics model used a frequency dependent structural damping function that is not consistent with modal damping coefficients measured in hammer tests.[4] Finally, although the comparisons of simulated single-point pressure spectra within the cavity compare very favorably to measurements, we have no direct means of validating the pressure loading on the store. Errors in store load distributions could also lead to errors

in store response. Further measurements incorporating multiple store-mounted pressure transducers or pressure-sensitive paint would be invaluable for further validation of the loads.

	x-accel	y-accel	z-accel
$M = 0.80$	17.2	20.0	1.5
$M = 1.47$	7.5	7.3	2.5

Table 5. Estimate of statistical convergence error (%) in RMS of simulated store aft accelerations.

VI. Conclusions

Coupled fluid/structure simulations of a compressible flow over a cavity containing a model captive store have been performed and validated against wind tunnel data for pressure loading and store response. The store surface pressure data generated by the simulations have been used to investigate details of the store loading for free stream Mach numbers of 0.60, 0.80, and 1.47. The major obsevervations from this work include:

- The hybrid RANS/LES simulation method used in this work is able to accurately reproduce measured single point cavity wall pressure spectra to within 2-3 dB in amplitude and 5% in frequency for most resonant cavity tone peaks, for both subsonic and supersonic Mach numbers. The simulations are also able to capture the changes in pressure spectra that occur when the store is added to the empty cavity.
- The prediction of store accelerations using the coupled fluid-structure simulations shows some success in calculating both natural and forced responses of the store. Uncertainties due to inadequate statistical convergence, not including the proper mode-dependent damping in the structural dynamics model, and perhaps in the details of the spatio-temporal pressure loading on the store may be responsible for inaccurate predictions for some frequencies and flow conditions.
- Examination of integrated forces and moments on the model store reveals a complex relationship between resonant cavity tones and resulting forces on the store. This may be due to the fact that the store interferes with the cavity shear layer in the present configuration, raising the possibility of loading from pressure disturbances within the shear layer itself, in addition to loading from the cavity tones. Further analysis of the simulation results is warranted to identify the loading mechanisms.

References

[1]J. E. Rossiter. Wind-tunnel experiments on the flow over rectangular cavities at subsonic and transonic speeds. Aeronautical Research Council Reports and Memoranda No. 3438, 1964.

[2]R. E. Dix and R. C. Bauer. Experimental and theoretical study of cavity acoustics. Technical Report AEDC-TR-99-4, 2000.

[3]J. L. Wagner, S. J. Beresh, J. Henfling, R. Spillers, and J. Blecke. Simultaneous vibration and acoustic measurements of a store in a compressible open cavity flow. AIAA-2013-0228, 51st AIAA Aerospace Sciences Meeting, 2013.

[4]J. L. Wagner, K. M. Casper, S. J. Beresh, P. S. Hunter, R. W. Spillers, J. F. Henfling, and R. L. Mayes. Experimental investigation of fluid-structure interactions in compressible cavity flows. AIAA-2013-3172, 2013 AIAA Fluid Dynamics Conference, San Diego, CA, 2013.

[5]J. Shipman, S. Arunajatesan, P. A. Cavallo, R. Birkbeck, and N. Sinha. Flow control for enhanced store separation. AIAA-2007-1239, 2007.

[6]C. J. Coley and A. J. Lofthouse. Correlation of weapon bay resonance and store unsteady force and moment loading. AIAA-2012-0415, 2012.

[7]S. Arunajatesan, M. Ross, M. Barone, and T. Garrett. Validation of an FSI modeling framework for internal captive carriage applications. AIAA Paper 2013-2157, 2013.

[8]M. M. Rai. Navier-Stokes simulations of blade-vortex interaction using high-order accurate upwind schemes. AIAA 87-0543, 1987.

[9]P. R. Spalart, M. L. Shur, M. Kh. Strelets, and A. K. Travin. Sensitivity of landing-gear noise predictions by large-eddy simulation to numerics and resolution. AIAA-2012-1174, 2012.

[10]S. Arunajatesan and M. Sinha. Hybrid RANS-LES modeling for cavity aeroacoustics predictions. *Int. J. Aeroacoustics*, 2(1):65–91, 2003.

[11]S. Arunajatesan, M. Bhardwaj, W. C. Riley, and M. Ross. One-way coupled fluid structure simulations of stores in weapons bays. AIAA-2013-0665, 2013.

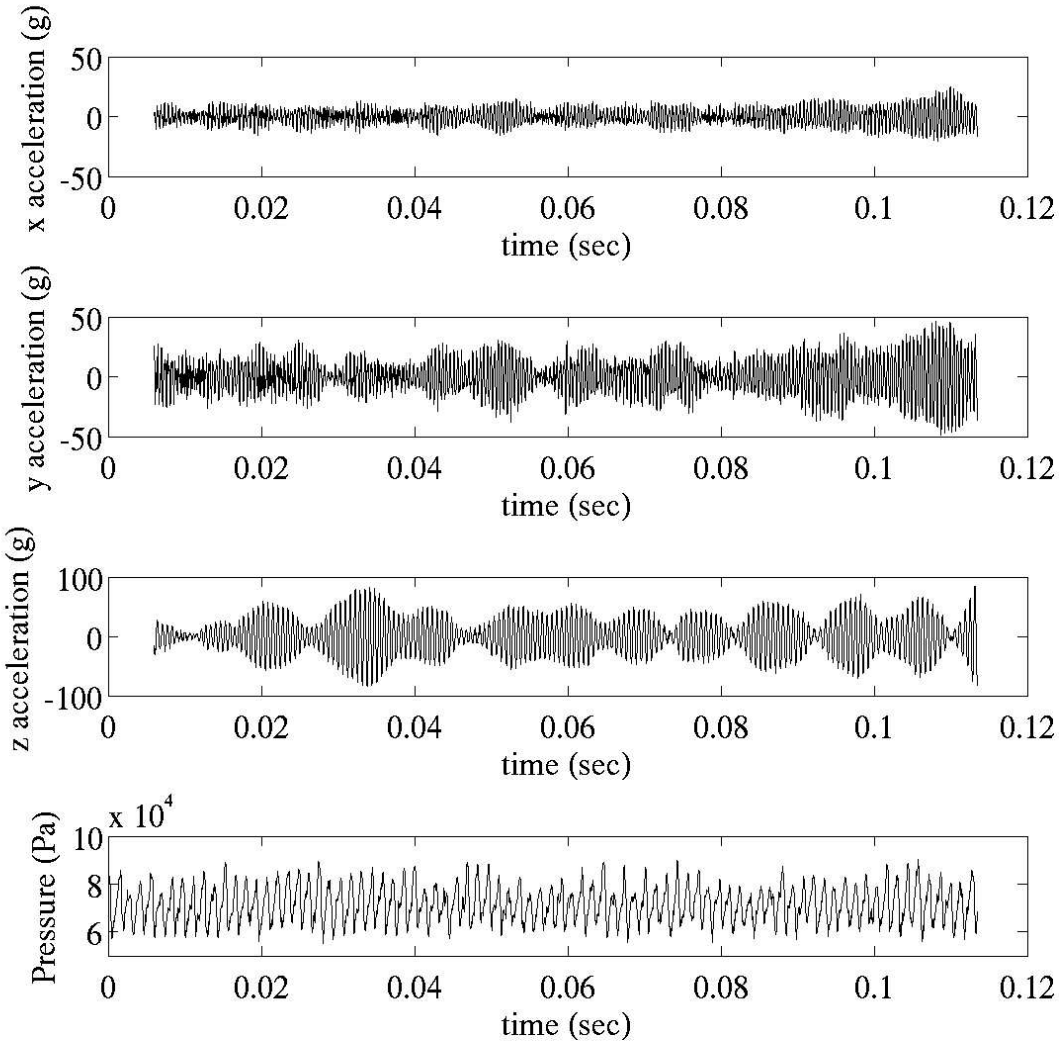

Figure 12. Acceleration time history at the aft store accelerometer location (A2), along with aft cavity wall pressure time history, $M = 0.80$.

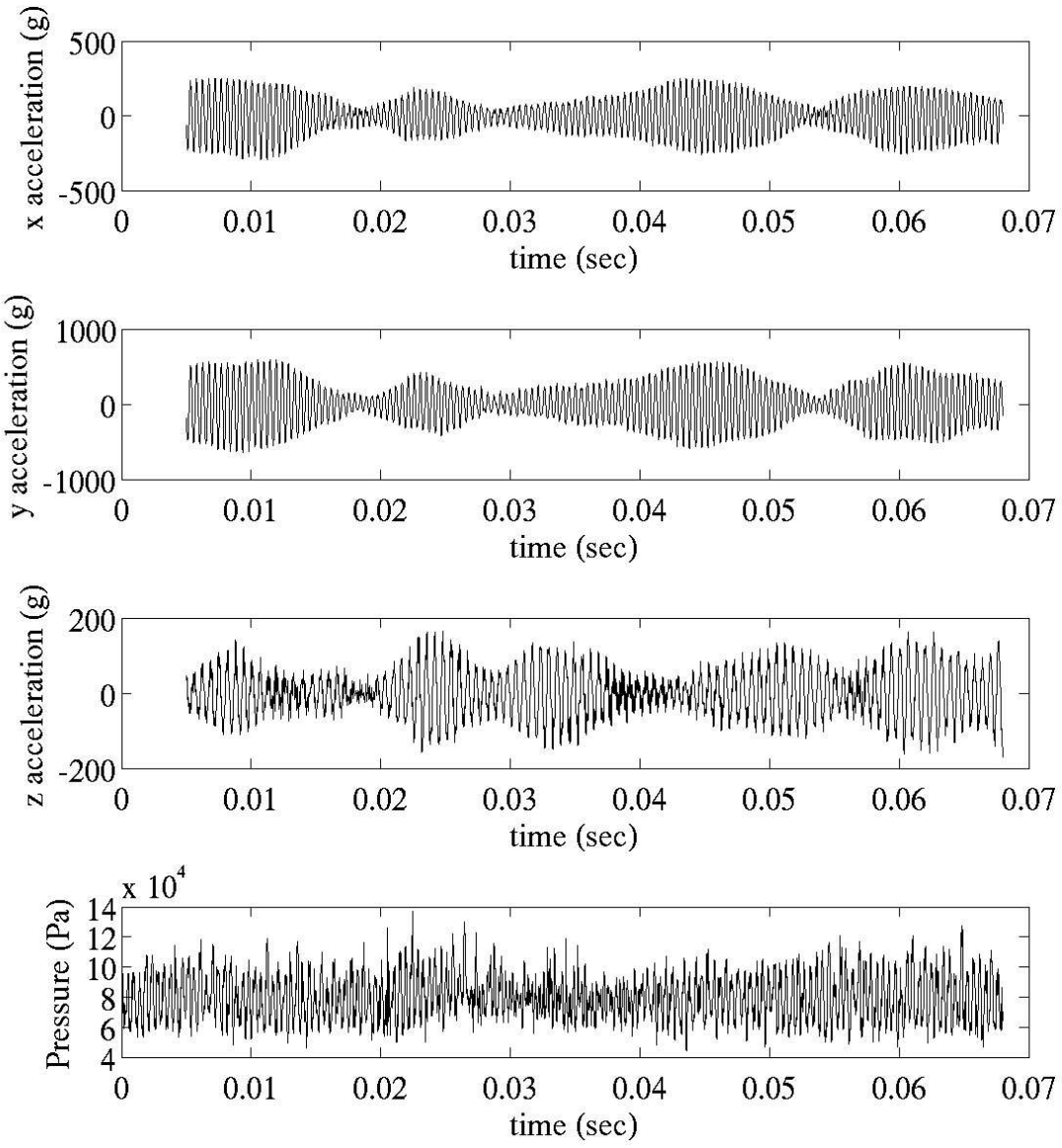

Figure 13. Acceleration time history at the aft store accelerometer location (A2), along with aft cavity wall pressure time history, $M = 1.47$.

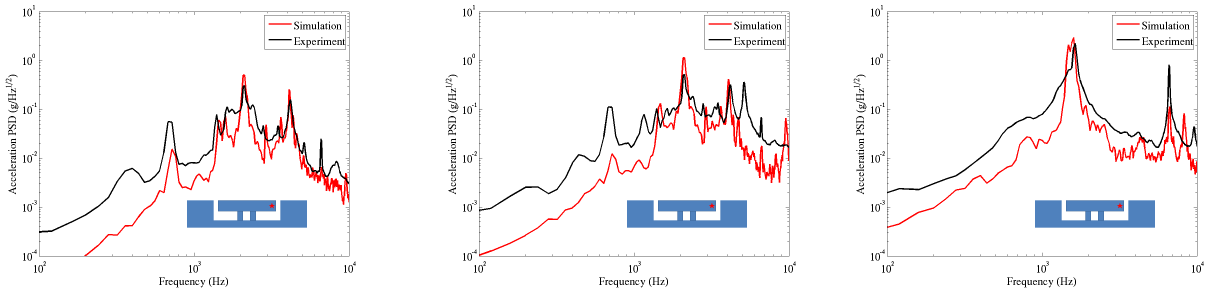

(a) x-acceleration. **(b)** y-acceleration **(c)** y-acceleration

Figure 14. Aft Store Acceleration PSD, Mach = 0.8.

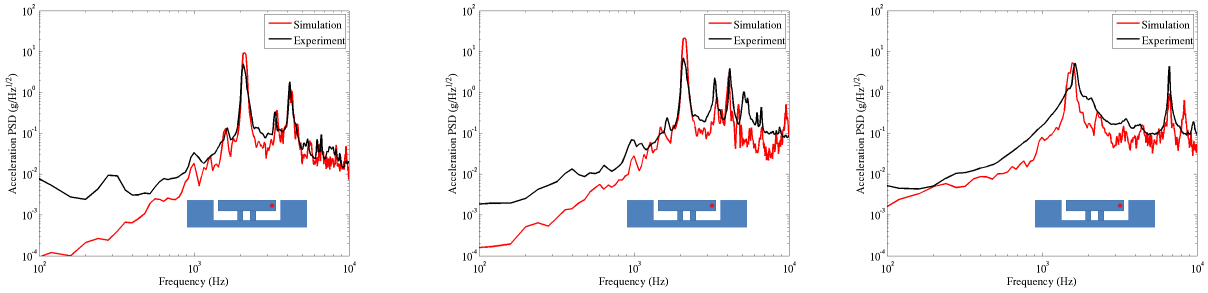

(a) x-acceleration. **(b)** y-acceleration **(c)** y-acceleration

Figure 15. Aft Store Acceleration PSD, Mach = 1.5.